Aerosol and cloud property relationships for summertime stratiform clouds in the northeastern Atlantic from Advanced Very High Resolution Radiometer observations

Mark A. Matheson, James A. Coakley Jr., and William R. Tahnk

College of Oceanic and Atmospheric Sciences, Oregon State University, Corvallis, Oregon, USA

[1] Advanced Very High Resolution Radiometer (AVHRR) 4-km data collected over the northeastern Atlantic off the coast of the Iberian Peninsula for May to August 1995 were used to investigate the feasibility of empirically deriving estimates of the aerosol indirect radiative forcing. A retrieval scheme was used to derive cloud visible optical depth, droplet effective radius, cloud layer altitude, and pixel-scale fractional cloud cover. A two-channel aerosol retrieval scheme was used to determine aerosol optical depth in cloud-free pixels. Mean aerosol optical depths derived from the cloud-free pixels in $1° \times 1°$ latitude-longitude regions on a given satellite overpass were associated with mean cloud properties derived from the cloudy pixels in the same region for the same satellite overpass. The analysis was restricted to $1°$ regions that contained only single-layered, low-level cloud systems. Because aerosol and cloud properties are highly variable, results for the 4-month period were composited into $5° \times 5°$ latitude-longitude regions and averaged to obtain reliable trends in the cloud properties as functions of aerosol burden. Consistent with expectations for the aerosol indirect effect, in some $5°$ regions, droplet effective radii decreased, and cloud visible optical depths increased as aerosol optical depths increased. The hypothesis that drizzle is suppressed in polluted clouds predicts that liquid water path should increase as aerosol burden increases. In three of the thirteen $5°$ regions studied, the liquid water path increased as aerosol optical depth increased, but in none of the regions was the increase in cloud liquid water statistically significant. In the remaining regions, cloud liquid water remained constant or even decreased with increasing aerosol optical depth. In many of the $5°$ regions, the retrieved aerosol optical depth increased as the percentage of cloudy pixels increased. Consistent with expectations from adiabatic cloud parcel models, droplet effective radius, cloud optical depth, and cloud liquid water path also increased as fractional cloud cover increased. The simultaneous increase in retrieved aerosol and cloud optical depths with increasing fractional cloud cover might have been due to the aerosol indirect effect, but it might also have resulted from processes that affect both the cloud and aerosol properties as cloud cover changes. The dependence on fractional cloud cover suggests that some of the trends between aerosol optical depth and the cloud properties cannot be solely attributed to the effects of the aerosols. For comparison with previous studies, the simultaneous changes in aerosol and cloud properties were used to estimate the daily average aerosol indirect forcing for overcast conditions in the summertime northeastern Atlantic. The magnitude of the indirect forcing relative to that of the direct forcing reported here is smaller than estimates reported by others.

1. Introduction

[2] The effect of particulates on clouds and their consequent effect on the sunlight reflected by clouds was first noted by *Twomey* [1974] and is known as the "Twomey Effect" or aerosol indirect radiative forcing. Starting with *Kaufman and Nakajima* [1993], several studies have used satellite imagery data to deduce the effect of aerosols on clouds by correlating aerosol and cloud properties within localized regions [*Kaufman and Fraser*, 1997; *Wetzel and Stowe*, 1999; *Nakajima et al.*, 2001; *Sekiguchi et al.*, 2003; *Quaas et al.*, 2004]. Among the goals of these studies were (1) to provide evidence for cloud-aerosol interactions on

regional and global scales, and (2) to empirically derive estimates of the aerosol indirect effect which might limit the large uncertainty in model estimates of the aerosol indirect radiative forcing. Partly because they rely on climate model simulations of cloud properties, which are known to be poor [*Randall et al.*, 2003; *Potter and Cess*, 2004], model estimates of the indirect forcing are highly uncertain [*Lohmann and Feichter*, 1997; *Rotstayn*, 1999; *Lohmann et al.*, 2000; *Lohmann and Lesins*, 2002]. The model estimates lead to the "poor confidence" and large uncertainty associated with the aerosol indirect radiative forcing as assessed by the *Intergovernmental Panel on Climate Change* [2001].

[3] Here the strategy of correlating aerosol properties with collocated cloud properties to deduce the indirect effect of aerosols was reexamined by analyzing NOAA 14 4-km AVHRR observations of marine stratus and stratocumulus and aerosol burden in the northeastern Atlantic for the summer of 1995. The region and season were selected because (1) stratus and stratocumulus are the dominant cloud system and (2) the flow is sufficiently weak that frequent intrusions of polluted air from Europe encroach on the marine environment [*Brenguier et al.*, 2000a]. Also, the NOAA 14 satellite was launched in December 1994 and the radiometric calibration of the AVHRR visible channel has been characterized for the summer of 1995 [*Tahnk and Coakley*, 2001a, 2001b]. Although AVHRR has fewer spectral bands and coarser resolution than currently available with the Moderate Resolution Imaging Spectrometer (MODIS) [e.g., *King et al.*, 2003], the AVHRR was used because of the multiyear length of its data record, which will be exploited in a forthcoming paper (M. A. Matheson et al., Satellite observations of summertime stratocumulus collocated with aerosols in the northeastern Atlantic, submitted to *Journal of Geophysical Research*, 2005).

[4] This satellite study differs from the previous satellite assessments in a variety of ways. First, the aerosols and the clouds were collocated at the same time in relatively small regions (1° × 1° latitude-longitude). This condition of simultaneity and collocation avoided the possibility of aerosols occurring on one day in one location being compared with cloud properties on another day in another location as was possible in some of the earlier studies [*Wetzel and Stowe*, 1999; *Sekiguchi et al.*, 2003]. Likewise, the relatively small region in which the clouds and aerosols were collocated also avoided attributing the appearance of a cloud response in one location to the effects of aerosols in another location [*Sekiguchi et al.*, 2003; *Quaas et al.*, 2004]. Second, results from the simultaneous occurrence of clouds and aerosols were composited within relatively limited geographic regions (5° × 5° latitude-longitude). Again, the restriction avoided comparisons of clouds in geographic regions subject to heavy aerosol burdens accompanied by one set of thermodynamic conditions with clouds in other geographic regions subject to light aerosol burdens accompanied by possibly distinctly different thermodynamic conditions as could have arisen in the global surveys performed by *Nakajima et al.* [2001] and *Sekiguchi et al.* [2003]. Third, only regions with single-layered, low-level, maritime clouds were examined in order to avoid multilayered cloud systems, which might have contaminated the results in the earlier studies.

[5] In this study, the cloud properties were retrieved using a scheme that accounts for the partial cloudiness of the pixels [*Coakley et al.*, 2005]. While some earlier studies sought to avoid pixels that were partially cloud covered [*Wetzel and Stowe*, 1999; *Nakajima et al.*, 2001], the retrieval schemes relied on the assumption that the pixels used to obtain the cloud properties were overcast. Such retrievals generally lead to estimates for partly cloudy pixels of cloud droplet effective radii that are larger and optical depths that are smaller than would be obtained if the pixels were overcast [*Han et al.*, 1994; *Platnick et al.*, 2003]. Consequently, as a region fills with clouds and the number of partly cloudy pixels decreases, cloud droplet effective radius might decrease while optical depth increases simply because of the biases in cloud properties associated with the assumption of overcast pixels. As aerosol optical depth has been found to increase with increasing cloud cover [*Sekiguchi et al.*, 2003; *Ignatov et al.*, 2005; *Loeb and Manalo-Smith*, 2005], correlations between aerosol burden and the biased retrieved cloud properties that arise as cloud cover increases could be misinterpreted as evidence of the Twomey Effect. The partly cloudy pixel retrieval scheme used here yields droplet radii and cloud optical depths that are both smaller, but only slightly so, for the clouds in the partly cloudy pixels when compared with those of clouds in nearby overcast pixels and is therefore less susceptible to trends that would mimic those associated with the Twomey Effect. Nonetheless, as is shown in section 4, cloud properties also vary systematically with regional cloud cover in ways that mimic expectations based on adiabatic cloud parcel models. Consequently, some of the trends between cloud properties and aerosol burden might be attributable to the response of the clouds to thermodynamic processes.

2. Cloud and Aerosol Properties

[6] Global Area Coverage (GAC) radiances, with a nominal nadir resolution of 4 km, measured by the Advanced Very High Resolution Radiometer (AVHRR) on board the National Oceanic and Atmospheric Administration (NOAA) satellite, NOAA 14, were analyzed for the months of May through August of 1995. All daytime satellite overpasses from the 4 months were used. The analysis area chosen for this study was in the northeastern Atlantic bounded by 35°–55°N latitude and 20°W–0° longitude. Although the region includes parts of Europe, cloud and aerosol properties were retrieved only over the ocean. The study region contained both coastal and open ocean regions. In addition, periods of both sustained onshore and offshore flow were observed in the NCEP reanalysis wind fields. These geographic and meteorological conditions allow for the analysis of a wide range of aerosol burdens and their effects on clouds. This region has also been studied in a variety of field campaigns such as the Atlantic Stratocumulus Transition Experiment (ASTEX) [*Albrecht et al.*, 1995] and the Second Aerosol Characterization Experiment (ACE−2) [*Raes et al.*, 2000].

[7] Channel 1 (0.64 μm) of the AVHRR was calibrated in reference to the radiometrically stable ice sheets of Antarctica [*Tahnk and Coakley*, 2001a, 2001b]. An on-board blackbody and deep-space views were used to calibrate channels 3 and 4 (3.7 and 11 μm) [*Kidwell*, 1995]. Imager pixels containing land were identified by the latitude and

longitude included in the AVHRR data stream and were removed from further analysis. Pixels which may have been affected by sun glint were assumed to be those for which the angle of reflection was within 40° of that for specular reflection from a flat surface. Pixels in the sun glint were removed from the analysis. A scene identification scheme was used to determine if the 4-km pixels were cloud-free, completely overcast by clouds in a single layer, partially covered by clouds, or overcast by clouds that were distributed in altitude [Coakley et al., 2005].

[8] Aerosol optical depths at 0.55 μm were retrieved in the imager pixels identified as cloud-free using a two-channel method originally developed to obtain aerosol properties from AVHRR for the Indian Ocean Experiment (INDOEX) [Coakley et al., 2002]. For the INDOEX aerosols, the bias and RMS error in the aerosol optical depth at 0.65 μm were 0.01 ± 0.06 when compared to surface Sun photometer data. While the retrieval scheme for the aerosols differentiated between a fine mode aerosol, an average continental aerosol described by Hess et al. [1998], and a coarse mode aerosol, a marine aerosol, the correlations performed here were between cloud properties and total aerosol optical depth, which is given by the sum of the fine and coarse mode aerosol optical depths. The total aerosol optical depth yielded the strongest correlations with cloud droplet effective radius. As the fine mode fraction for the region was found to be 0.66, the fine mode optical depth and total aerosol optical depth produced much the same correlations with droplet effective radius, while the coarse mode optical depth produced little correlation. Nonetheless, in all but one of the 5° latitude-longitude regions for which the correlations were significant when using both the total aerosol optical depth and the fine mode optical depth, or using both the total optical depth and the coarse mode optical depth, the trends in the cloud properties with aerosol optical depth were in the same direction.

[9] Cloud properties were retrieved using the method of Coakley et al. [2005]. For pixels that the scene identification scheme identified as being overcast by optically thick single-layered clouds, radiances at 0.64, 3.7 and 11 μm were used to retrieve cloud optical thickness, droplet effective radius, and cloud layer altitude. For partly cloudy pixels the clouds were assumed to be at the mean altitude retrieved for the nearby overcast pixels. In addition, the pixel radiances were assumed to have a linear mixture of the radiances that would be seen if the pixels were either completely overcast or completely cloud-free, so that,

$$I = (1 - A_c)I_s + A_cI_c(\tau_c, R_e, z_c)$$

where I is the radiance observed by the satellite instrument, A_c is the fractional cloud cover for the pixel, I_s is the average radiance for the cloud-free portion of the pixel, and $I_c(\tau_c, R_e, z_c)$ is the average radiance for the cloud-covered portion of the pixel and is a function of: τ_c, the cloud optical depth, R_e, the droplet effective radius, and, z_c, the cloud layer altitude. With z_c given by the altitude retrieved for nearby pixels that were overcast, radiances at 0.64, 3.7, and 11 μm were used to derive A_c, τ_c, and R_e. Radiances in the cloud-free portions of the partly cloudy pixels were assumed to be equal to the mean of the radiances taken from nearby cloud-free pixels, or, lacking sufficient nearby

cloud-free pixels, from a monthly and regional climatology of cloud-free radiances.

[10] An example of derived cloud and aerosol properties is shown in Figure 1. The region was covered largely by low-level clouds (Figure 1a) but some high clouds were present on this day as indicated by their emission at 11 μm (Figure 1b). As described below, $1° \times 1°$ latitude-longitude regions that contain clouds that are not from single-layered, low-level systems were excluded from the data analysis. On this day, there was a high aerosol burden in the region off the Iberian Peninsula, but the air north of approximately 43° N was relatively clean (Figure 1c). If the aerosol properties in the cloudy pixels are assumed to be similar to the aerosol properties in the nearby cloud-free pixels then the clouds off the coast of Iberia were in an environment with high aerosol burden, whereas the clouds further north were in an environment with a relatively low aerosol burden. The clouds in the north had larger droplet radii and the clouds near the coast of Iberia had smaller droplet radii (Figure 1d). The relationship between droplet radius and aerosol burden illustrated in Figure 1 is qualitatively consistent with that expected for the Twomey Effect.

[11] The analysis in this study was limited to single-layered, low-level clouds. Regions off the western coast of most continents at midlatitudes often contain marine boundary layer clouds and are regions likely to be susceptible to cloud-aerosol interaction [Nakajima et al., 2001]. Screening rules were applied to the radiances and retrieved cloud properties within $1° \times 1°$ latitude-longitude regions to identify regions in which all of the clouds were part of a single-layered, low-level system. If a cloud layer was present in the region, the mean cloud temperature and the 5th percentile of the 11-μm brightness temperature were required to be within 20 K of the mean surface temperature. In addition, to ensure that the clouds were in a well-defined layer, as opposed to being distributed in altitude, if the difference between the mean surface temperature and the mean cloud temperature was greater than or equal to 10 K then $(T_s - T_{5th})/(T_s - T_c) < 1.2$ and $\sigma_c/(T_s - T_c) < 0.2$, where, T_s is the mean surface temperature, T_{5th} is the 5th percentile of the 11-μm brightness temperature, T_c is the mean temperature associated with the layer at altitude z_c, and σ_c is the standard deviation of T_c, for the 1° latitude-longitude region. If $T_s - T_c < 10$ K then the requirements were $T_s - T_{5th} < 12$ K and $\sigma_c < 2$ K.

[12] Figure 2 illustrates the average properties of single-layered, low-level clouds for the region under study. Satellite data for individual cloud or aerosol properties were averaged in $1° \times 1°$ latitude-longitude regions for each orbital pass. In the case of the cloud properties, the averages were obtained by weighting the values by the pixel-scale fractional cloud cover. The means of each 1° latitude-longitude region were then averaged over all passes. For the summer of 1995, the air in the northeastern Atlantic was more polluted near the coast and cleaner over the ocean (Figure 2a). The cloud droplet effective radius of single-layered, low-level clouds was small near the coast and large over the open ocean (Figure 2b). Aerosol optical depth increased and cloud droplet effective radius decreased from west to east, as if the trends were manifestations of the Twomey Effect. On the other hand, the thinning and breakup of clouds as the continent is approached is typical
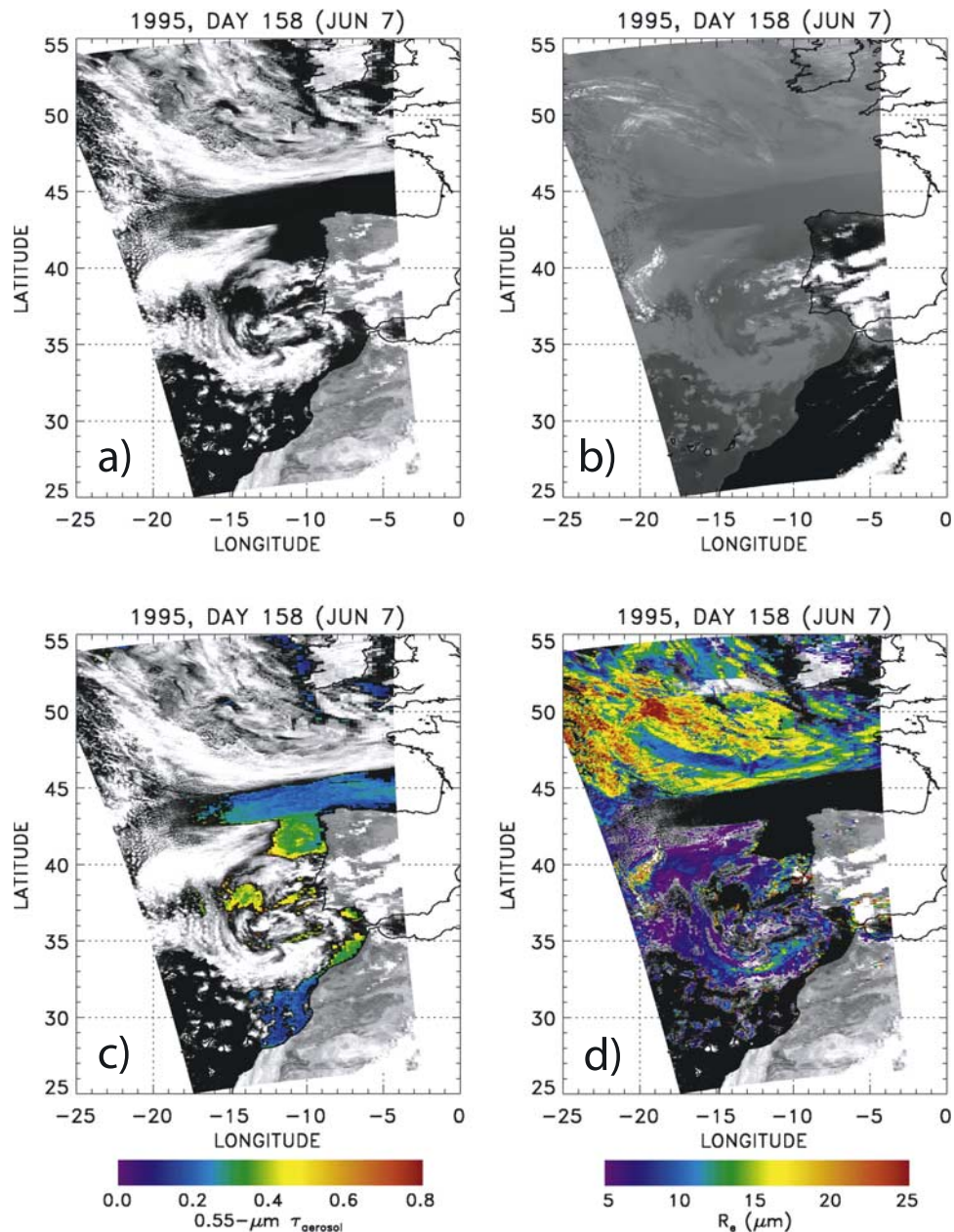
Figure 1. Images of the study region on 7 June 1995, dominated by low-level, single-layered stratocumulus off the west coast of Europe. (a) 0.84-μm 4-km AVHRR reflectances. (b) 11-μm radiances. Upper-level clouds (light objects) overlie a portion of the low-level clouds. (c) Same as Figure 1a but overlain with 0.55-μm aerosol optical depth. (d) Same as Figure 1a but overlain with droplet effective radius (μm).

of marine stratus and may simply reflect the influence of incursions of dry continental air in the marine boundary layer and not the Twomey Effect. Regions closest to the coast were usually clear or contained broken clouds and more extensive cloud cover appeared further from shore (Figure 2c).

[13] Fractional cloud cover was relatively constant from south to north (Figure 2c). Both aerosol optical depth and cloud droplet radius increased from south to north despite the supposition that cloud-aerosol interaction should result in smaller droplets where there is more aerosol. Droplet effective radius did not decrease as aerosol optical depth increased from south to north because there were south-north trends in cloud optical depth (Figure 2d) and liquid water path (Figure 2e), here calculated as $W = \frac{2}{3} R_e \tau_c \rho$, where $\rho = 1$ g cm^{-3} is the density of water.

3. Relating Collocated Aerosol and Cloud Properties

[14] Pixel-scale observations from each satellite overpass were mapped into $1° \times 1°$ latitude-longitude regions. As stated earlier, all data were screened to ensure that $1°$ latitude-longitude regions that were either cloud-free
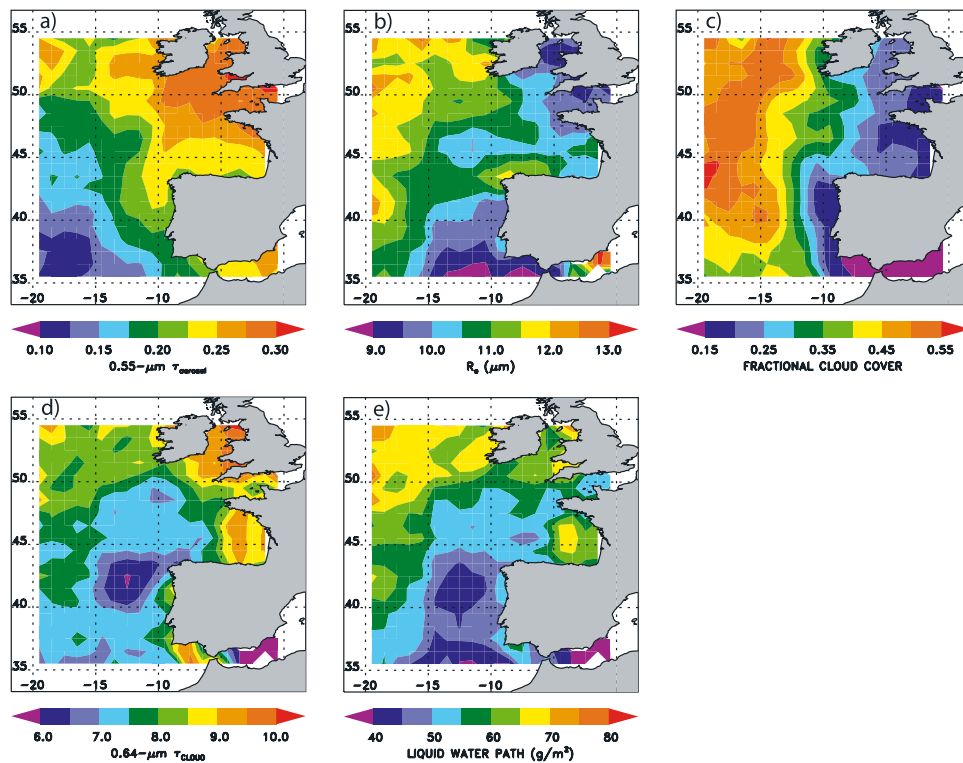
Figure 2. Summertime (May to August 1995) average properties of single-layered, low-level clouds and aerosols. Contour data have been smoothed to show large-scale trends. (a) 0.55-μm aerosol optical depth. Aerosol data from $1° \times 1°$ latitude-longitude regions that contained clouds that were not part of a single-layered, low-level cloud system were not included in the analysis. (b) Droplet effective radius (μm). (c) Fractional cloud cover. (d) 0.64-μm cloud optical depth. (e) Liquid water path (g/m^2). In Figures 2b−2e, data were limited to $1°$ latitude-longitude regions that contained only low-level, single-layered cloud systems. In calculating the pass averages within a region, cloud properties were weighted by the pixel-scale fractional cloud cover.

ocean or partly covered by nothing but single-layered, low-level clouds were the only regions included in the analysis. The means of all cloud and aerosol properties were calculated in each $1°$ latitude-longitude region with the constraint that a minimum of 10 pixels or 5% of the pixels in the region (whichever was greater) for both aerosol and cloud properties were required. Because aerosol optical depth has an autocorrelation length of roughly 100 km [*Anderson et al.*, 2003], the aerosol properties in the cloud-free pixels of the region were assumed to be well correlated with the aerosol properties in the cloudy pixels of the same region.

[15] Within a geographic region, cloud properties and aerosol burden vary markedly from day to day. To detect reliable trends in cloud properties and aerosol burden the effects of the variability are reduced through averaging. In this study observations for the $1°$ latitude-longitude regions for each orbital pass were averaged within their corresponding $5° \times 5°$ latitude-longitude regions and then the pass averages were averaged for the 4-month period. In addition, as was discussed in the previous section, there were large-scale trends in the $20° \times 20°$ latitude-longitude region that could be interpreted as evidence for the Twomey Effect. The trends in cloud properties, on the other hand, may not be due to changes in aerosol burden but instead due to other factors such as the outflow of

dry air from the continent. Averaging the collocated cloud and aerosol properties for the $1°$ latitude-longitude regions within the $5°$ latitude-longitude regions reduces somewhat the influence of the large-scale geographic gradients. Of course, gradients are still likely within the $5°$ latitude-longitude regions, but the $5°$ regions were the smallest studied because of the relatively small number of samples that fell into each region.

[16] For each satellite overpass, the observations were segregated into 0.05-unit-wide bins in 0.55-μm aerosol optical depth. The means of the cloud properties and the corresponding aerosol optical depths were then calculated for each bin. After the means of each bin for each pass had been calculated, the bins were averaged over all passes. For example, Figure 3 shows the mean droplet effective radius calculated for every 0.05-unit-wide bin of aerosol optical depth. In Figure 3, and all subsequent figures, results for all sixteen $5°$ latitude-longitude regions are displayed simultaneously in their appropriate geographic location. Results for regions that contained land used data only from the pixels identified as being over ocean. In order to ensure that the values in each season-averaged bin were representative, means from at least five different passes for that bin were required. Linear least squares fits were performed to quantify the trends in the cloud properties with aerosol optical depth. To improve the confidence in the least squares fits,
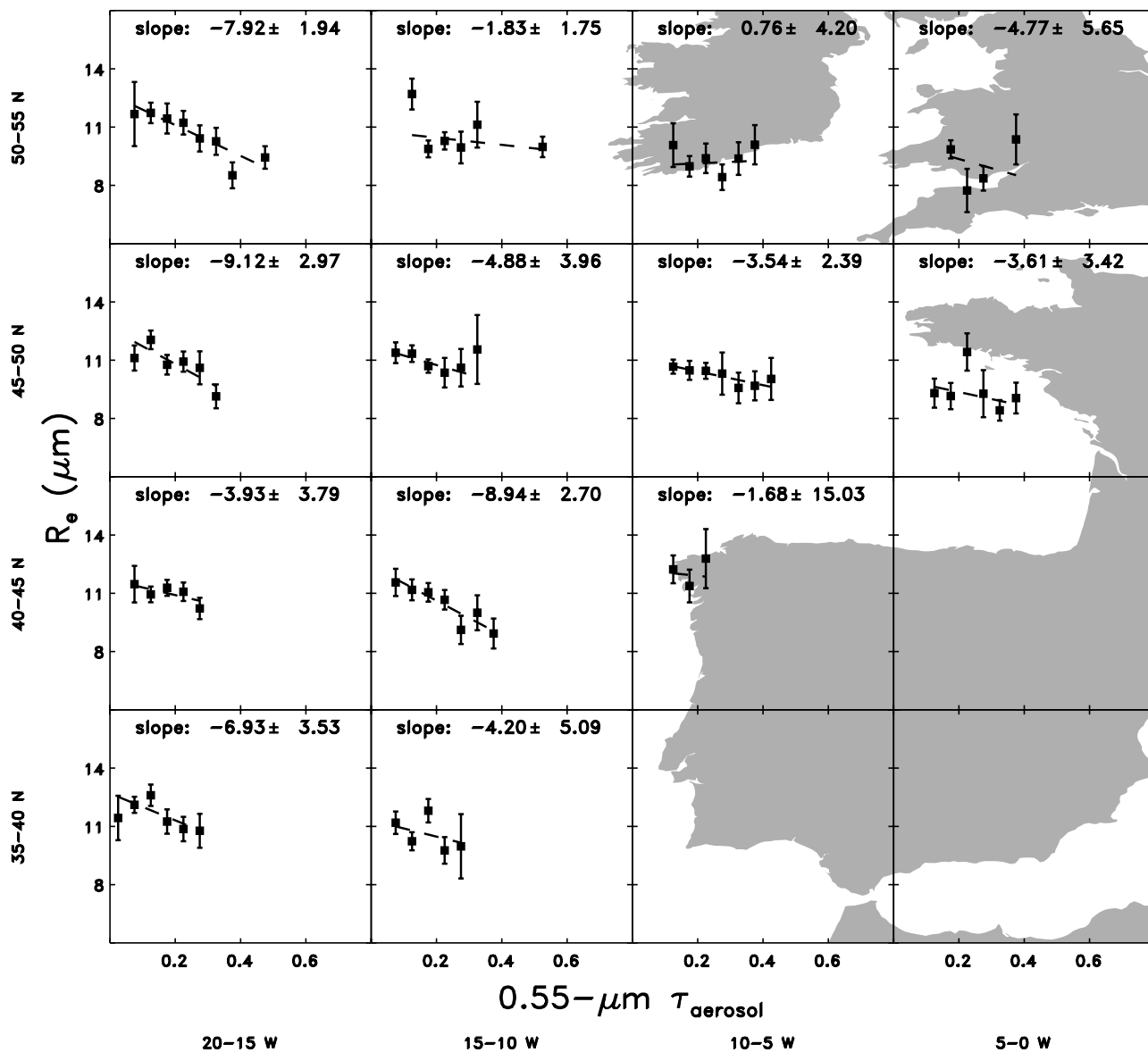
Figure 3. Means of daily averaged droplet effective radius (μm) for 1° latitude-longitude regions binned for each 0.05 interval of aerosol optical depth. Each subpanel contains data from that 5° × 5° latitude-longitude region. Error bars represent the standard error, given by the standard deviation of the means from individual days for that bin divided by the square root of the number of days that contributed observations to that bin. The dashed line is a linear fit to the bin means inversely weighted by the standard errors. Also given are the mean and standard deviation estimated for the slope of the linear fit.

outlier data were removed by eliminating 1° latitude-longitude regions from individual satellite passes that had means that were outside the 5th and 95th percentiles for any property, except fractional cloud cover, in that 5° latitude-longitude region for the entire summer's collection of data. Fractional cloud cover is constrained between 0.0 and 1.0, so extremes were not considered outliers. Three of the sixteen regions had insufficient observations for calculating correlations. These regions are left blank in Figures 3–9.

[17] The error bars for each bin in Figure 3 are given by the standard error of the bin, calculated as the standard deviation of the means of the individual satellite passes contributing to that bin divided by the square root of the number of satellite passes. Averages within a bin

for each pass were taken to be statistically independent. As noted earlier, linear fits to the bin means were performed to determine the trends in the cloud properties with aerosol optical depth. In the fits, the means were inversely weighted by their estimated standard errors [*Bevington*, 1969]. The slopes and estimates of their uncertainties were obtained from the distribution of the data about the trend lines [*Press et al.*, 1994] and are reported in the figures. A slope is considered to be statistically significant if its magnitude is greater than twice the estimated uncertainty.

[18] For the 4-month period, 577 satellite overpasses were analyzed. There were 59,352 1° latitude-longitude regions that contained at least one pixel that was ob-
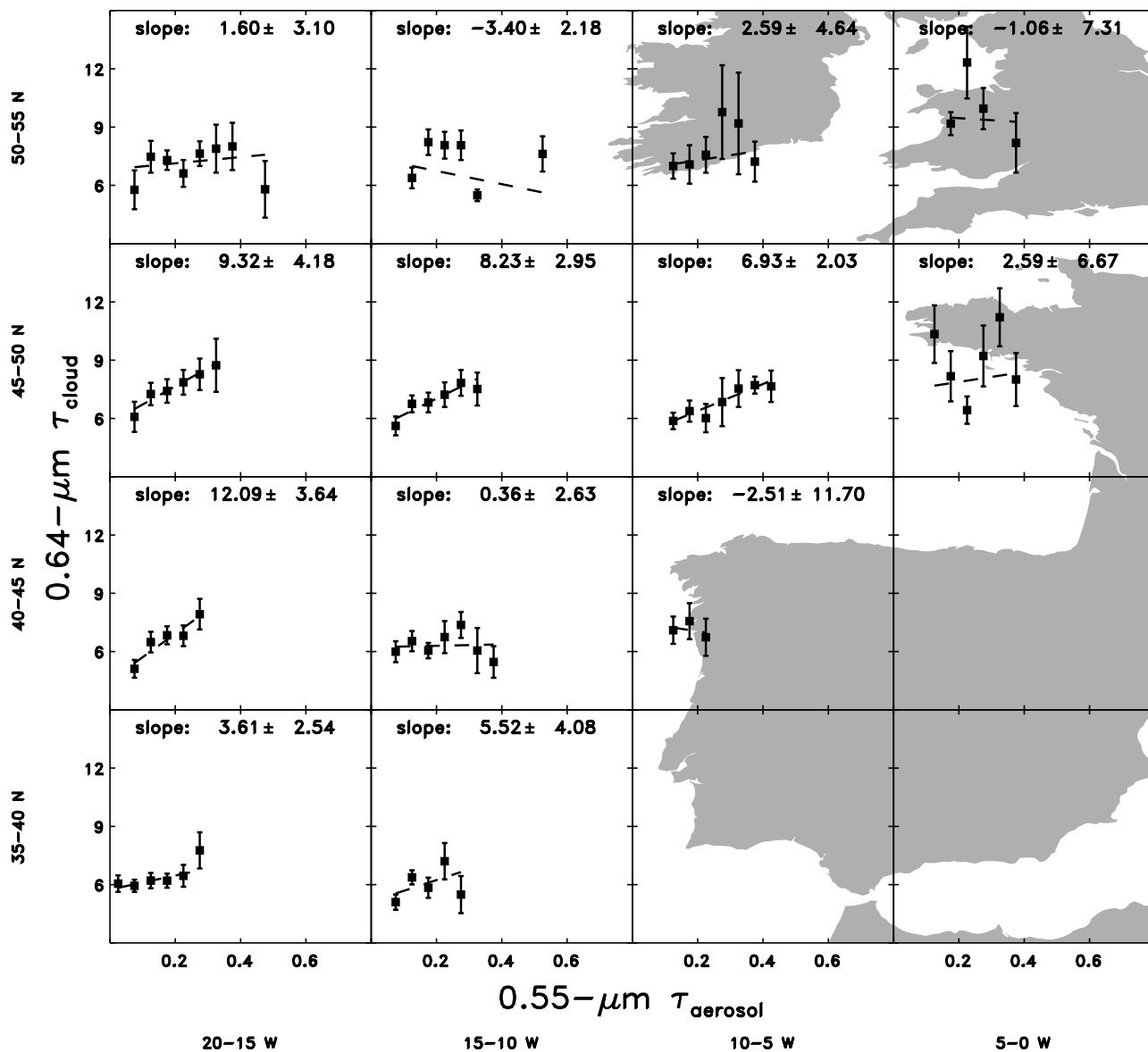
Figure 4. Same as Figure 3 but for 0.64-μm cloud optical depth and 0.55-μm aerosol optical depth.

served during daytime, over water, and away from sun glint, and was therefore suitable for attempting a retrieval. The number and percentage of 1° regions that passed the data screening algorithms described in this section are listed in Table 1. In order to maximize the signal of the aerosol indirect effect, data were tightly screened. Only 2.9% of the available 1° regions were used in the analysis. Despite the screening, the data were still rather noisy. The estimated uncertainties in the slopes of the associated cloud properties and aerosol optical depths were often larger than the slope estimates themselves. The highly variable nature of clouds makes determining reliable trends in cloud properties challenging.

[19] As is shown in Figure 3, in all but one of the 5° latitude-longitude regions droplet radius decreased as aerosol burden increased. Some regions showed an increase in cloud optical depth as aerosol burden increased while other regions showed no trend or even a decrease in cloud optical depth as aerosol burden increased

(Figure 4). Eight of the thirteen regions showed a decrease in droplet effective radius and an increase in cloud optical depth as aerosol burden increased. In only one of these eight regions, however, were the slopes significantly greater than twice the estimated error in the slopes and thus taken to be statistically significant. All but one region showed an increase in droplet number concentration, as given by $\tau_c/(2\pi R_e^2)$, with increasing aerosol burden (not shown). Clouds in some regions were probably gaining CCN as aerosol burden increased and the clouds were probably responding to the aerosols consistent with the Twomey Effect.

[20] None of the 5° latitude-longitude regions showed an increase in liquid water path as aerosol burden increased with an estimated slope that was significantly larger than the error estimate of the slope (Figure 5). Many regions showed a decrease in liquid water path as aerosol burden increased. Decreases in liquid water have also been observed for ship tracks [Platnick et al., 2000;
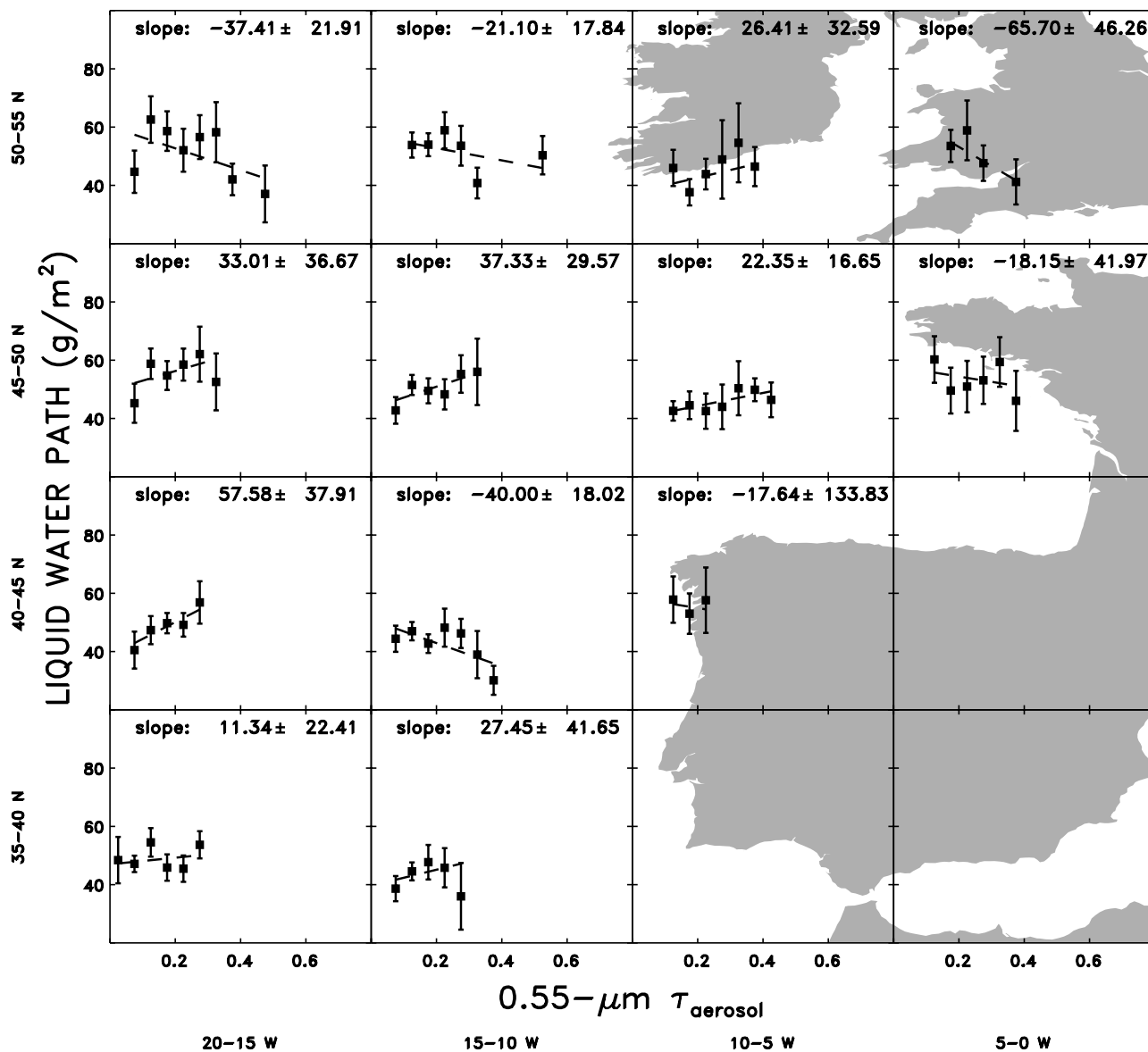
Figure 5.   Same as Figure 3 but for cloud liquid water path (g/m^2) and 0.55-μm aerosol optical depth.

Coakley and Walsh, 2002]. Such trends might stand as evidence against the suppression of drizzle and increased cloud liquid water and cloud lifetimes for polluted clouds proposed by *Albrecht* [1989]. On the other hand, high aerosol burdens in the coastal regions might have been associated with air originating over the continent, and thus the air was dryer. Clouds that formed in this dryer air might have been starved for water and quickly evaporated by entraining dry air from above the cloud, while clouds that formed far from the coast might have formed in moister, oceanic air with higher humidity and were less likely to dry out [*Ackerman et al.*, 2004]. Attempts to use humidity data from 2.5° × 2.5° latitude-longitude resolution NCEP reanalysis products to test this hypothesis were inconclusive. The decrease in cloud liquid water as aerosol burden increased might also be explained by the aerosol semidirect effect; an increase in aerosol burden might lead to increased atmospheric heat-

ing which hinders cloud formation and augments cloud dissipation [*Ackerman et al.*, 2000].

4.   Dependence of Cloud Properties and Aerosol Optical Depth on Regional Cloud Cover

[21]   The previous section demonstrated that in some regions changes in cloud and aerosol properties were related in ways that are consistent with the Twomey Effect. Cloud properties, on the other hand, are also interrelated regardless of aerosol burdens. The possibility that the relationships among the cloud properties could have been incorrectly attributed to the Twomey Effect is explored.

[22]   Adiabatic cloud models provide a theoretical basis for relationships among cloud properties. *Szczodrak et al.* [2001] derive $R_e \propto \tau_c^{1/5}$ and give observational evidence for this relationship in maritime stratus off the west coast of North America. *Brenguier et al.* [2000b] describe aircraft
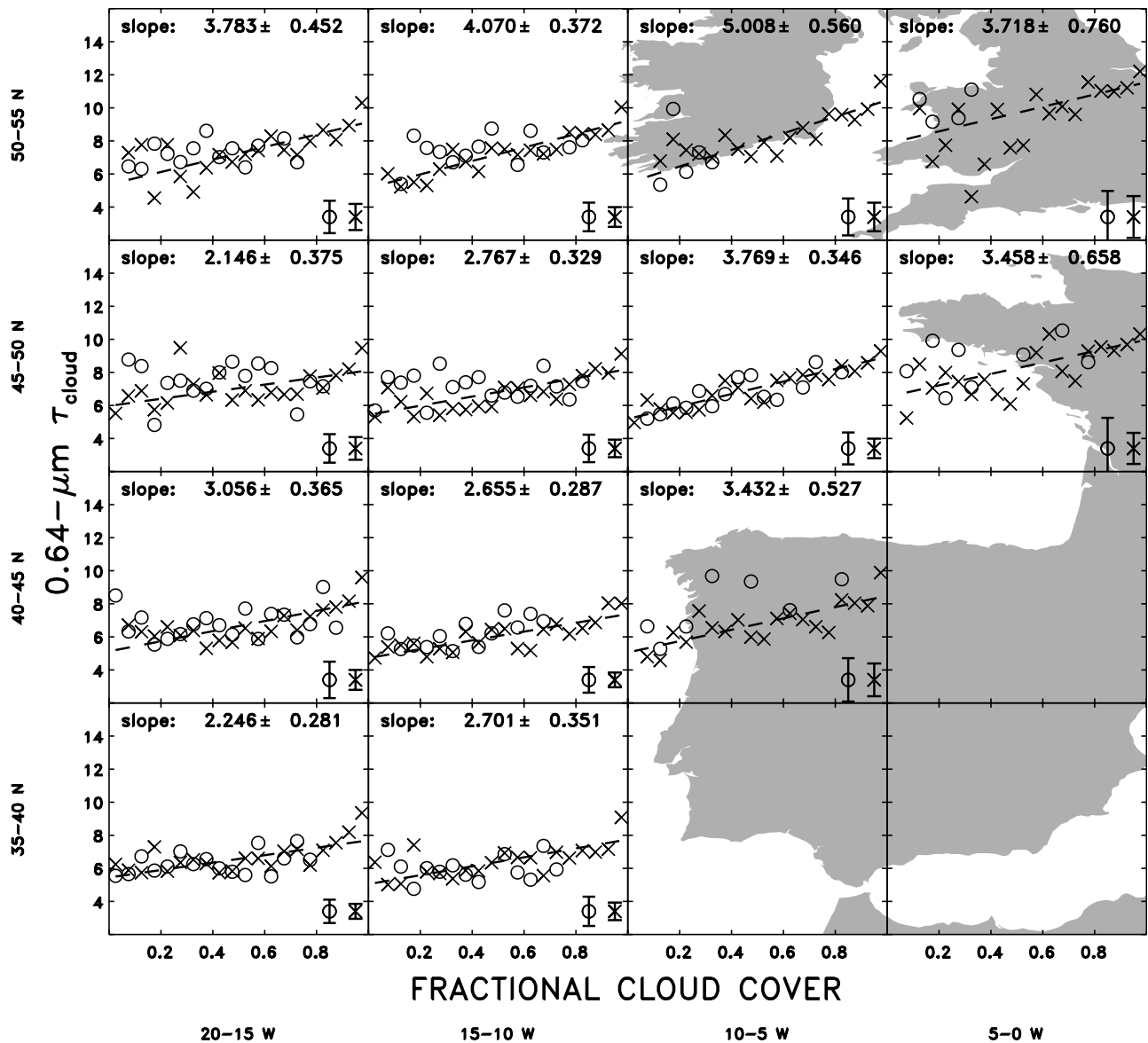
Figure 6. Means of daily averaged 0.64-μm cloud optical depth for 1° latitude-longitude regions binned for each 0.05 interval of fractional cloud cover. Each subpanel contains data from that 5° × 5° latitude-longitude region. Circles are data for 1° regions that contained sufficient observations of both aerosol and cloud properties to be included in Figures 3−5. Crosses are data from 1° latitude-longitude regions that passed the screening tests for single-layered, low-level clouds but lacked a sufficient number of aerosol retrievals to be included in the aerosol-cloud associations. The root-mean-square of the standard error (as described in Figure 3) for the two data sets are shown in the bottom right corner of each panel. The dashed line is a linear fit to the bin means of the combined data sets inversely weighted by the standard errors of the combined data sets. Also given are the mean and standard deviation estimated for the slope of the linear fit.

observations showing liquid water content, $w \propto h$, where h is height above cloud base. By integration, the column water amount, $W \propto H$, where H is cloud geometric thickness. *Brenguier et al.* [2000b] also provide observational evidence for the derived relationship $R_e \propto h^{1/3}$, and find $\tau_c \propto H^{5/3}$. All of these relationships are for constant cloud droplet number concentration, and should therefore be observable for adiabatic conditions and a given aerosol burden. As cloud fields break up, however, fractional cloud cover decreases, mixing of dry air into clouds increases, and

the relationships among cloud properties are likely to depart from those derived assuming adiabatic cloud parcels.

[23] Figures 6 and 7 show trends in cloud properties as fractional cloud cover increased. Here binning procedures similar to those used in Figures 3−5 were used but the bins are for every 0.05 in fractional cloud cover for the 1° regions. When associating aerosol and cloud properties, the 1° latitude-longitude regions used in the analysis were required to contain both cloud and aerosol retrievals. This restriction does not apply when comparing cloud properties
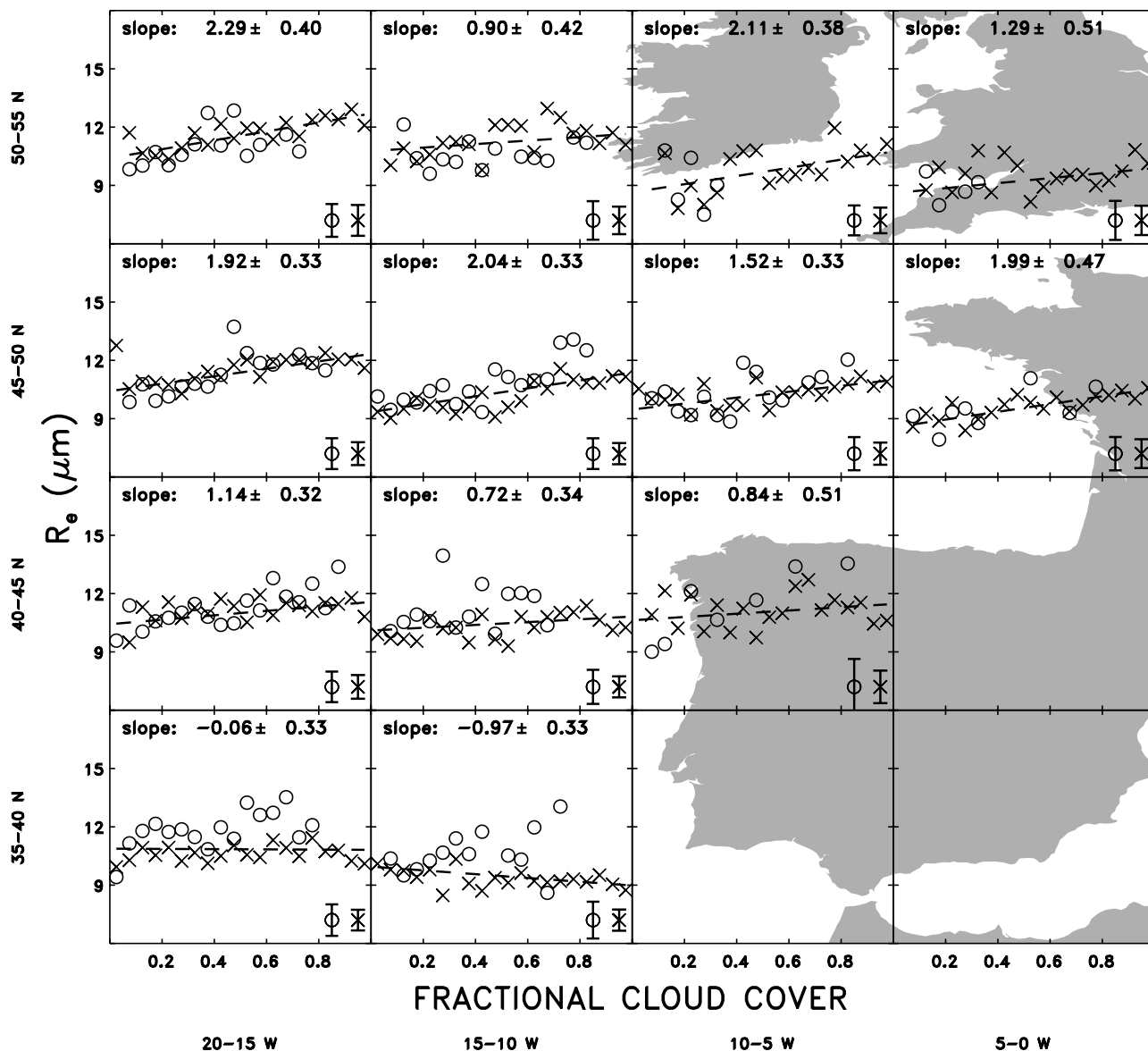
Figure 7. Same as Figure 6 but for droplet effective radius (μm) and fractional cloud cover.

to fractional cloud cover. Figures 6 and 7 show data from both 1° latitude-longitude regions that were used in the cloud-aerosol associations (circles) and 1° latitude-longitude regions that passed the screening tests for single-layered, low-level clouds but lacked sufficient numbers of aerosol retrievals to be included in the cloud-aerosol associations (crosses). The data shown as circles in Figures 6 and 7 are the same as used in the cloud-aerosol correlations (Figures 3–5). As regions filled with clouds, the relationships among the cloud properties exhibited qualitatively the tendencies expected for adiabatic cloud parcels. Cloud optical depth increased as fractional cloud cover increased (Figure 6). In all but the southernmost regions, droplet effective radius increased as fractional cloud cover increased (Figure 7). For a given cloud cover fraction, cloud optical depths and droplet effective radii of the clouds associated with (circles) and not associated with aerosols (crosses) showed little difference with the exception of droplet effective radius in the southernmost regions. There,

clouds observed near aerosols (circles in Figure 7) had larger droplet effective radii than clouds that were present with no collocated aerosol retrievals (crosses in Figure 7). Liquid water path, which is proportional to the product of cloud optical depth and droplet effective radius, increased as fractional cloud cover increased in all 5° latitude-longitude regions (not shown). Clouds observed near aerosols appeared to have higher cloud tops than clouds observed with no collocated aerosol retrievals (not shown). Cloud top height decreased with increasing fractional cloud cover in approximately half of the 5° latitude-longitude regions and was independent of fractional cloud cover in the other half of the regions (not shown).

[24] Aerosol optical depth can be associated with both the fractional cloud cover and the cloudy pixel fraction, defined as the fraction of pixels in a 1° latitude-longitude region that were identified as having clouds (pixel-scale cloud fraction, $A_c > 0.2$). Because aerosol optical depth is not retrieved in partly cloudy pixels, cloudy pixel fraction was used as an
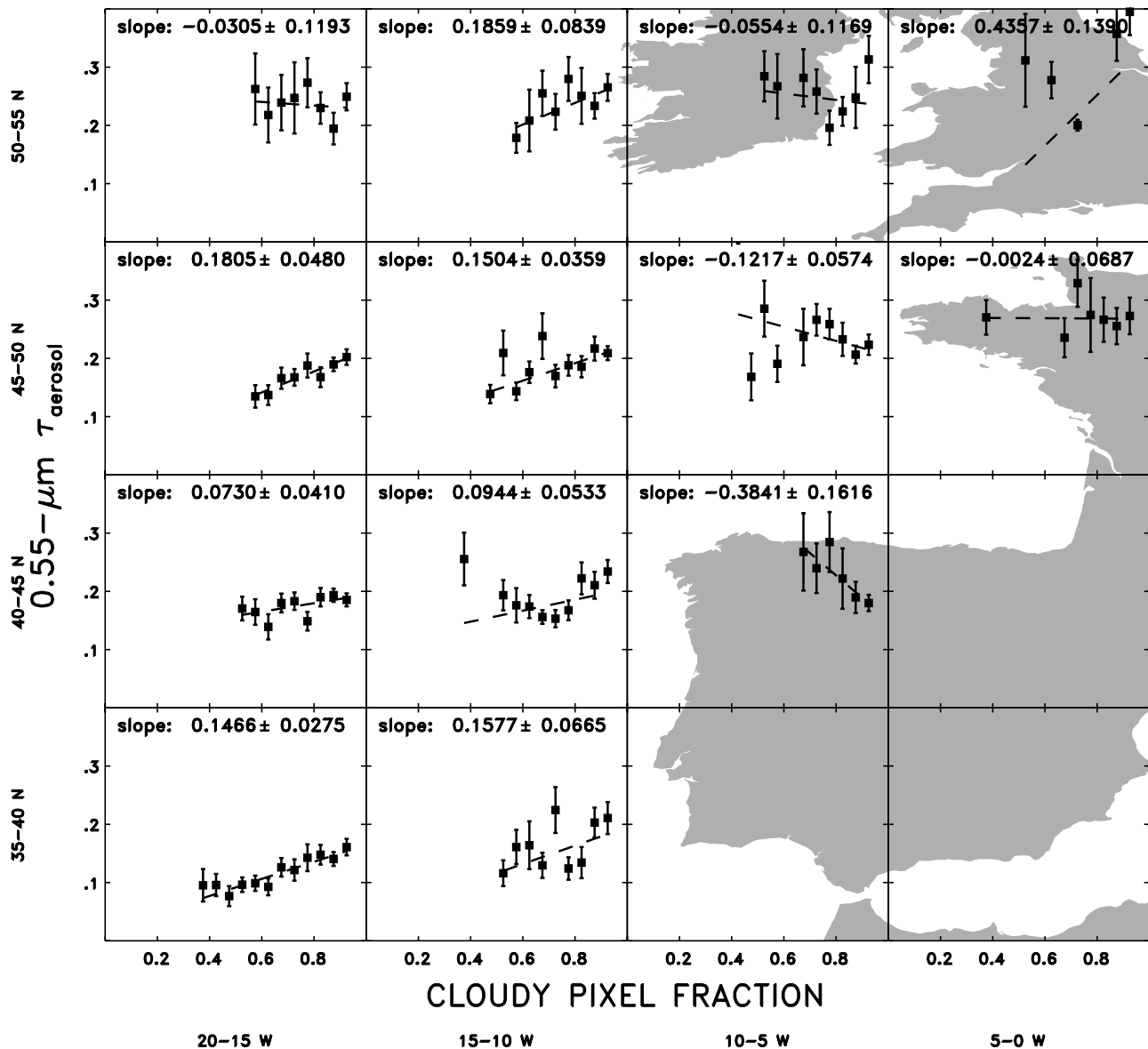
Figure 8. Same as Figure 3 but for 0.55-μm aerosol optical depth and cloudy pixel fraction. Cloudy pixel fraction is the fraction of pixels within a 1° latitude-longitude region that were identified as containing clouds (pixel-scale cloud fraction, $A_c > 0.2$).

index of regional cloud cover. Cloudy pixel fraction is similar to the fractional cloud cover derived using threshold cloud retrievals [*Coakley et al.*, 2005]. Retrieved aerosol optical depth increased as cloudy pixel fraction increased in many of the 5° latitude-longitude regions (Figure 8). This increase in aerosol optical depth as cloudy pixel fraction increased may be due to cloud contamination. A single AVHRR GAC pixel is approximately 1 km × 4 km at nadir [*Kidwell*, 1995]. Some pixels identified as being cloud-free may have contained subpixel resolution clouds. These unidentified clouds caused the retrieved aerosol optical depths to be erroneously high. Presumably, subpixel-scale clouds are more common in the presence of detectable clouds, explaining the trend toward larger aerosol optical depth as cloudy pixel fraction increased. Better algorithms for detecting subpixel-scale resolution clouds and higher

pixel resolution would both help alleviate this source of error.

[25] The apparent increase in aerosol burden with increasing cloud cover could also be caused by the swelling of aerosol particles in the vicinity of clouds. Clouds form in environments with high relative humidity and aerosol particles swell as relative humidity increases [*Seinfeld and Pandis*, 1998; *Clarke et al.*, 2002]. Other causes for the apparent increase in aerosol optical depth as cloud cover increases include: increased illumination of the aerosols by sunlight leaving the sides of nearby clouds [*Podgorny*, 2003], increased particle production near clouds [*Kütz and Dubois*, 1997], and an increase in aerosol size due to in-cloud processing of CCN [*Lelieveld and Heintzenberg*, 1992]. Clearly, characterizing how aerosols change and ensuring that cloud contamination of the "cloud-free"
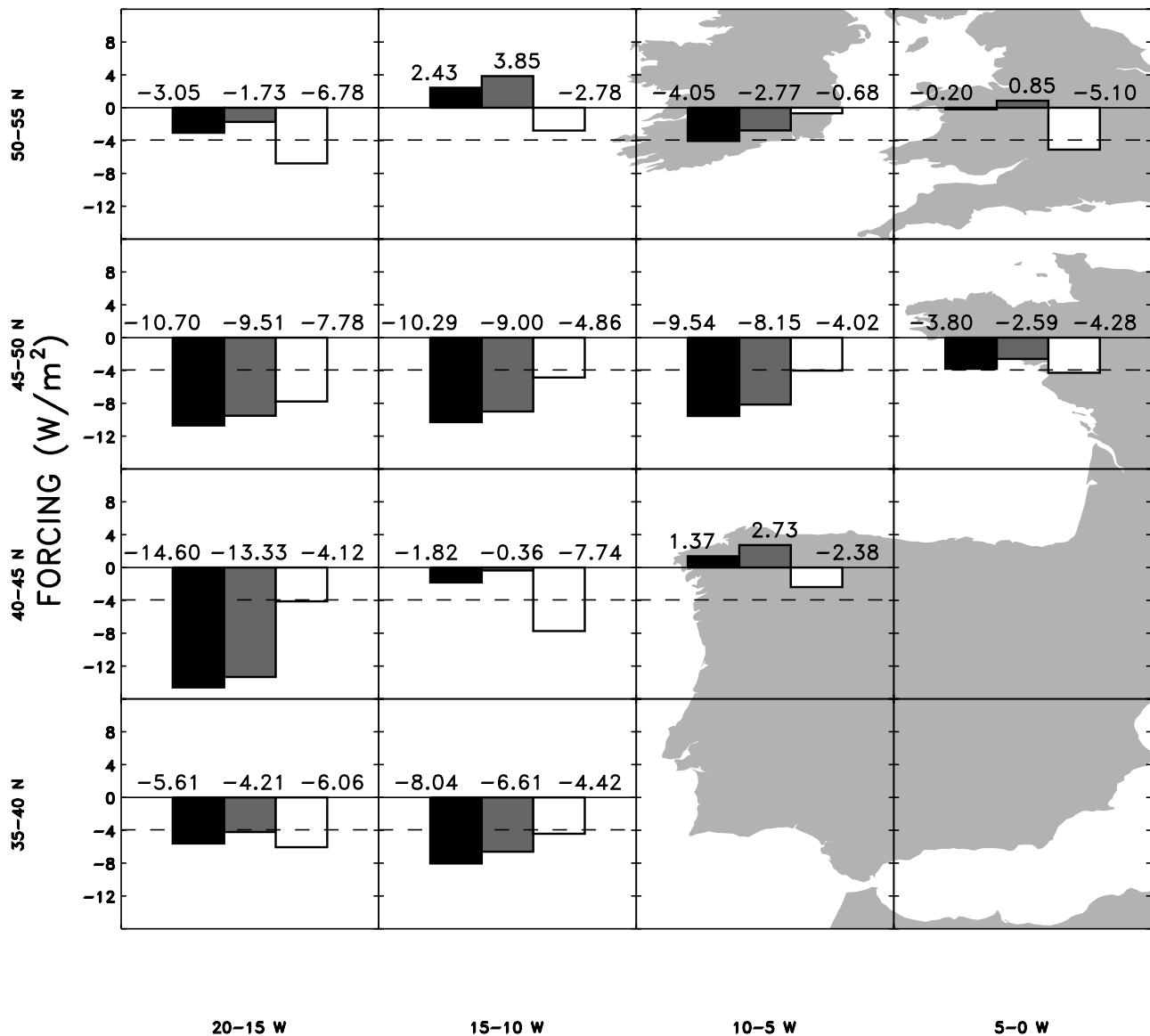
Figure 9. Radiative forcing estimates (W/m²) for an arbitrary increase of 0.55-µm aerosol optical depth of 0.1 (from 0.15 to 0.25). Solid bars are the forcings for overcast conditions calculated using the changes in cloud optical depth taken from the linear fits in Figure 4 and an increase of the aerosol optical depth below the cloud. Shaded bars are the same forcing as the black bars except the aerosol optical depth was held at the "background" level. Open bars are the forcings for overcast conditions calculated using the changes in droplet effective radius taken from the linear fits in Figure 3 and assuming a constant liquid water path. The dashed line is the aerosol direct radiative forcing for cloud-free conditions (−3.94 W/m²).

pixels remains unchanged as regions go from being largely cloud-free to largely overcast are hurdles which will have to be overcome before reliable assessments of the indirect effect of aerosols can be obtained empirically. Better cloud screening and better characterizations of aerosols in the vicinity of clouds are among the desired outcomes of the combination of lidar and imagery to come from *CALIPSO* and A-Train observations [*Winker et al.*, 2003].

[26] In all of the 5° latitude-longitude regions where aerosol optical depth increased as cloudy pixel fraction increased (Figure 8), cloud optical depth also increased as fractional cloud cover increased (Figure 6). The simultaneous increase in cloud and aerosol optical depth could be interpreted as an indication of the Twomey Effect, as suggested previously in this study (Figure 4). On the other hand, both cloud and aerosol optical depth might have been changing in response to cloud cover, indicating that at least some of the perceived correlation between cloud and aerosol optical depths may not be due to the Twomey Effect.

[27] How can aerosol optical depth (Figure 8) and droplet effective radius (Figure 7) both increase with increasing cloud cover fraction, yet droplet effective radius decrease with increasing aerosol optical depth (Figure 3)? The results shown for all of the parameters in Figures 3–8 are means drawn from widely dispersed distributions. Aerosol and

Table 1. Number and Percentage of $1° \times 1°$ Latitude-Longitude Regions That Survived Successive Data Screening Tests[a]

	Aerosol		Cloud	
Screening	Number	%	Number	%
At least 10 pixels or 5% (whichever was greater) of all pixels in region had cloud (aerosol) retrievals	11,806	19.9	30,286	51.0
Region contained only cloud-free pixels or clouds from single-layered, low-level cloud systems	9,620	16.2	16,820	28.3
Region contained cloud and aerosol properties that were within the 5th and 95th percentile for that 5° latitude-longitude area	7,963	13.4	11,697	19.7
Region contained both cloud and aerosol retrievals that passed previous data screening tests	1,930	3.3	1,930	3.3
At least 5 cloud retrievals per 0.05-unit-wide bin of aerosol optical depth in at least 3 separate bins for that 5° latitude-longitude area	1,741	2.9	1,741	2.9

[a]Percentages are based on 59,352 1° latitude-longitude regions from 577 satellite overpasses that contained at least one pixel that was observed during daytime, over water, and away from sun glint, and was therefore suitable for attempting a retrieval.

cloud optical depths have highly skewed distributions. Both have long tails stretching to large optical depths at low frequencies. Droplet radius, on the other hand, has a more compact distribution owing to bounds constrained by droplet formation at the low end and by precipitation at the high end. The full range of cloud properties is exhibited under average aerosol conditions while the clouds that appear with the infrequent occurrence of large aerosol burdens tend to have smaller than average droplets and, for the most part, larger than average optical depths. The fact that droplet radius decreases with increasing aerosol optical depth despite the countering trends of increasing droplet radius and aerosol optical depth with increasing cloud cover fraction suggests that the clouds are likely responding to the increased particle loading. On the other hand, since the number of partly cloudy pixels generally decreases and the number of overcast pixels increases as regional cloud cover increases, and since droplet radius is generally overestimated when the partly cloudy pixels are assumed to be overcast, the downward trend in droplet radius with increasing aerosol optical depth may also arise from misidentifying some partly cloudy pixels as being overcast [*Coakley et al.*, 2005]. Because of the natural trends in cloud properties with changing cloud fraction, the potential errors in the cloud property retrievals, and the observed increase in aerosol optical depth as the cloudy pixel fraction increases, caution must clearly be used in attributing observed correlations of cloud and aerosol properties to the Twomey Effect.

5. Radiative Forcing Estimates

[28] Section 3 demonstrated that cloud microphysical properties might have been changing in response to changes in aerosol optical depth. Section 4 explained that the correspondence between aerosol optical depth and cloud properties is more complicated than suggested by section 3. Because of the great interest in determining the magnitude of aerosol indirect radiative forcing, this section estimates the forcing using the trends calculated in section 3. These results must, of course, be viewed skeptically in light of the discussion of section 4.

[29] A broadband radiative transfer model that accounts for scattering and absorption by gases, aerosols, and clouds [*Coakley et al.*, 2002] was used to calculate top of the atmosphere fluxes in each of the 5° latitude-longitude

regions. For the calculations, an equal mix of continental and marine aerosols as described by *Hess et al.* [1998] was assumed. The mean fraction of continental aerosol type for the 1° latitude-longitude regions containing both cloud and aerosol retrievals was 0.66 ± 0.30. In this study, an arbitrary change in 0.55-μm aerosol optical depth of 0.1 was used to produce the radiative effects. The "background" level was chosen to be an aerosol optical depth of 0.15, and the "polluted" level was chosen to be an aerosol optical depth of 0.25. When a cloud was inserted in the model it was placed above the aerosol layer and the optical depth of the cloud was taken from the linear fits in Figure 4 associated with the aerosol optical depths set at 0.15 and 0.25.

[30] Calculations were performed for five different cases: (1) cloud-free and a "background" 0.55-μm aerosol optical depth of 0.15, (2) overcast with a cloud optical depth given by that associated with a "background" 0.55-μm aerosol optical depth of 0.15 as given in Figure 4 combined with an underlying aerosol with the same optical depth, (3) cloud-free and a "polluted" 0.55-μm aerosol optical depth of 0.25, (4) overcast with a cloud optical depth associated with a "polluted" 0.55-μm aerosol optical depth of 0.25 as given in Figure 4 combined with an underlying aerosol with the same optical depth, and (5) overcast with a cloud optical depth associated with a "polluted" 0.55-μm aerosol optical depth of 0.25 as given in Figure 4 but combined with an underlying aerosol with the "background" 0.55-μm optical depth of 0.15. The difference between cases 1 and 3 is the aerosol direct radiative forcing and is the same in all 5° latitude-longitude regions. The difference between cases 2 and 4 is here reported as the aerosol indirect radiative forcing. Changes in cloud cover associated with changes in aerosol optical depth were not considered in these calculations. The aerosol indirect radiative forcing reported here is not comparable to the forcing between preindustrial and current times, but is rather the forcing that results from an arbitrary 0.1 change in the 0.55-μm aerosol optical depth for overcast conditions. Cases 2 and 5 had the same amount of aerosol, but the optical depths of the clouds were different. The difference between cases 2 and 5 was used to investigate the relative contributions of changes in cloud properties and changes in aerosol burden in the calculation of the aerosol indirect radiative forcing.

[31] The direct radiative forcing for cloud-free oceans is the same in all 5° latitude-longitude regions, -3.94 W/m^2

(shown as dashed lines in Figure 9). This forcing is the 24-hour average forcing for an increase of 0.1 in the aerosol 0.55-μm optical depth for cloud-free oceans during the summer months in the northeastern Atlantic. The indirect radiative forcing varied from −14.60 W/m^2 to 2.43 W/m^2 (shown as solid bars in Figure 9). In approximately half the regions, the indirect radiative forcing was found to provide more cooling than the direct radiative forcing. In two of the regions, the indirect radiative forcing was found to be warming. In these two regions, cloud optical depth decreased with increasing aerosol optical depth (Figure 4).

[32] Case 5 gives the top of the atmosphere forcing for "polluted" clouds over "background" aerosols. The difference between case 2 and case 5 is shown as shaded bars in Figure 9 and was compared to the aerosol indirect radiative forcing (the difference between case 2 and case 4) as an indication of how much of the aerosol indirect forcing was solely the result of the changes in cloud properties. In all regions, the aerosol indirect radiative forcing and the forcing by changes in cloud properties alone were similar, within 1.5 W/m^2, indicating that changes in the overcast regions due to the scattering and absorption by the increased burden of aerosols was relatively minor.

[33] The radiative forcing calculations were repeated, but instead of calculating cloud optical depth using the trends shown in Figure 4, cloud optical depth was calculated using the observed changes in droplet effective radius as aerosol optical depth increased (Figure 3) and an assumption of fixed liquid water. The indirect radiative forcing calculated in this manner was always cooling and varied from −7.78 to −0.68 W/m^2 (shown as open bars in Figure 9). The average value of the radiative forcing calculated for constant liquid water, weighting the 13 regions equally, was −4.69 W/m^2, which is smaller than the average forcing calculated using observed changes in cloud optical depth, −5.22 W/m^2. In ten of the regions the forcing calculated by assuming fixed liquid water is more than 3 W/m^2 different from the forcing calculated by using observed changes in cloud optical depth. In one region, the assumption of fixed liquid water gives a forcing that was 10.48 W/m^2 smaller than the value calculated using the observed changes in cloud optical depth. Many climate model simulations show an increase in cloud water content with increasing aerosols [e.g., *Feichter et al.*, 2004] whereas the results presented here show that a decrease in liquid water path is clearly possible (Figure 5).

[34] The mean value of the aerosol indirect radiative forcing for overcast conditions, weighting the 13 regions equally, was −5.22 W/m^2 for a 0.1 change in aerosol 0.55-μm optical depth. The change in albedo for overcast conditions per unit change in aerosol optical depth, calculated using a solar constant of 1365 W/m^2 and the diurnal average of the cosine of the solar zenith angle for July for the North Atlantic of 0.354, was $\Delta r / \Delta \tau_a = 0.11$. *Kaufman and Fraser* [1997], studying the effect of smoke on low-level clouds over the Amazon, observed a similar value, $\Delta r / \Delta \tau_a = 0.12 \pm 0.08$.

[35] *Sekiguchi et al.* [2003], using AVHRR data, estimated the global mean aerosol indirect radiative forcing, not including changes in cloud fraction, as between −0.7 and −0.9 W/m^2. Their fractional cloud cover was between 0.3 and 0.4, indicating an indirect radiative forcing for overcast conditions of −1.75 to −3.0 W/m^2. They also calculated an aerosol direct radiative forcing of −0.4 W/m^2, indicating a radiative forcing for cloud-free conditions of −0.57 to −0.67 W/m^2. Therefore *Sekiguchi et al.* [2003] calculated an indirect forcing for overcast conditions that was 3 to 4.5 times greater than the direct forcing for cloud-free conditions. In the current study, the mean value of the aerosol indirect radiative forcing for overcast conditions was only slightly larger than the direct forcing for cloud-free conditions (−5.22 and −3.94 W/m^2 respectively). When holding cloud liquid water constant, *Sekiguchi et al.* [2003] calculated an indirect radiative forcing (−0.64 or −0.16 W/m^2) that was 30 or 76% less than the indirect forcing calculated for observed changes in cloud optical depth (−0.91 or −0.68 W/m^2). The current study calculates an indirect radiative forcing assuming constant liquid water that was 10% less than the forcing calculated from observed changes in cloud optical depth (−4.69 and −5.22 W/m^2 respectively). Both *Sekiguchi et al.* [2003] and the current study indicate that the assumption of fixed liquid water can lead to estimates of the aerosol indirect radiative forcing that are different from the indirect forcing that is estimated for the observed changes in cloud optical depth.

[36] *Rotstayn and Penner* [2001] used a global climate model to estimate the global average direct radiative forcing between the preindustrial and current eras as −0.75 W/m^2 and the indirect forcing as −2.57 W/m^2. Because their model included multiple cloud layers (approximately 40% low-cloud cover and 32% high-cloud cover), it is difficult to translate these numbers into forcings for cloud-free and overcast conditions. Nevertheless, their estimate of indirect forcing was substantially larger than their estimate of direct radiative forcing. A major difference between the current study and those of *Sekiguchi et al.* [2003] and *Rotstayn and Penner* [2001] is that their studies were global averages whereas the current study was limited to a 20° × 20° latitude-longitude region in the northeastern Atlantic. In addition, the current study used collocated simultaneous observations of aerosol and cloud properties as discussed earlier.

6. Conclusions

[37] AVHRR imagery data with a nominal nadir resolution of 4 km were collected over the northeastern Atlantic for May to August 1995. Within each satellite overpass, mean cloud properties deduced from the cloudy pixels in 1° × 1° latitude-longitude regions were associated with simultaneous mean aerosol properties deduced from the cloud-free pixels in the same 1° latitude-longitude regions. The observations were screened so that 1° latitude-longitude regions that contained only single-layered, low-level clouds and had sufficient numbers of cloud-free pixels yielding aerosol retrievals were used in the analysis. In pixels that contained clouds, a retrieval scheme was used to derive: cloud visible optical depth, droplet effective radius, cloud layer altitude, and pixel-scale fractional cloud cover. Aerosol optical depth was retrieved in cloud-free pixels. Results were composited in 5° × 5° latitude-longitude areas. The conditions of simultaneity and close spatial proximity were adopted to ensure that the observed properties of the clouds were in response to the observed aerosol burden, that is,

comparisons of clouds from one day and location to aerosols from a different day or different location were avoided.

[38] Clouds in some areas of the study region appeared to respond to aerosols as predicted by the Twomey Effect: as aerosol optical depth increased, cloud droplet number concentration increased, droplet effective radius decreased, and cloud optical depth increased. Strong evidence for trends consistent with the Twomey Effect was lacking in many of the 5° latitude-longitude regions. Many regions exhibited no change or even a decrease in cloud liquid water as aerosol burden increased. The incursion of dry, polluted continental air in the marine environment is suggested as a possible explanation for the decrease in cloud water associated with the increase in aerosol optical depth.

[39] As regional fractional cloud cover increased, droplet effective radius, cloud optical depth, and cloud liquid water path all increased. Aerosol optical depth increased as the percentage of pixels identified as containing clouds (pixel-scale cloud fraction, $A_c > 0.2$) increased. The increase in retrieved aerosol optical depth as cloud fraction increased might have been due to (1) cloud contamination in the retrievals of the aerosol properties, (2) the swelling of aerosols in the high-humidity cloudy environments, (3) the increased illumination of the cloud-free columns by the scattering of sunlight reflected from nearby clouds, (4) the increased particle production by photochemical processes in the vicinity of clouds, and (5) the chemical processing within cloud droplets leading to larger particles when the droplets evaporate. The simultaneous increase in cloud optical depth and aerosol optical depth as fractional cloud cover increased might be interpreted as the aerosol indirect effect. On the other hand, cloud and aerosol optical depth were both responding to an increase in cloud cover and some of the correlation between the cloud and aerosol optical depths might not have been due to the Twomey Effect.

[40] An assumption intrinsic to all satellite studies of cloud-aerosol interaction is that clouds observed near aerosols are influenced by aerosols similar to those observed nearby. The current study was limited to single-layered, low-level clouds. It was assumed that most of the aerosols were in the boundary layer and affected the microphysical properties of the low-level clouds. The region off the coast of Europe was chosen, in part, because aerosol plumes coming from the continent are often in the boundary layer [*Johnson et al.*, 2000]. A vertical profiling instrument such as GLAS [*Abshire et al.*, 1998] or the lidar to be flown on the *CALIPSO* satellite [*Winker et al.*, 2003] is required to determine whether the observed clouds and aerosols are actually at the same altitude and thus likely to be interacting, or a substantial fraction of the aerosol is in a lofted layer above the clouds, as presumably would be the case for the long-range transport of windblown dust.

[41] For comparison with other studies, a broadband radiative transfer model was used to calculate the direct and indirect radiative forcing for an arbitrary change of 0.1 in the aerosol 0.55-μm optical depth. The 24-hour average summertime indirect radiative forcing calculated for overcast conditions in the 5° latitude-longitude regions ranged from −14.60 to 2.43 W/m^2. The majority of this forcing was due to changes in the cloud properties and not to the increased

reflectivity caused by increased aerosol burden beneath the clouds. When averaged over all regions, the aerosol indirect effect for overcast conditions was −5.22 W/m^2, which was only slightly larger than the direct radiative forcing of −3.94 W/m^2 for cloud-free regions. Rerunning the forcing calculations using the observed changes in droplet effective radius and assuming fixed liquid water resulted in an aerosol indirect radiative forcing that was 10% less (−4.69 W/m^2) than the forcing calculated from observed changes in cloud optical depth. The indirect forcing obtained here is similar to that found by *Kaufman and Fraser* [1997]. The indirect forcing when compared with the direct forcing is smaller than similar comparisons reported by *Sekiguchi et al.* [2003] and by *Rotstayn and Penner* [2001]. Here no account was made for changes in fractional cloud cover which may be associated with the effects of the aerosols because, as noted earlier, many alternative physical processes might explain the correlations observed between aerosol burden and cloud cover fraction.

References

Abshire, J. B., J. C. Smith, and B. E. Schutz (1998), The geoscience laser altimeter system (GLAS), *AIP Conf. Proc.*, *240*, 33–37.

Ackerman, A. S., O. B. Toon, D. E. Stevens, A. J. Heymsfield, V. Ramanathan, and E. J. Welton (2000), Reduction of tropical cloudiness by soot, *Science*, *288*, 1042–1047.

Ackerman, A. S., M. P. Kirkpatrick, D. E. Stevens, and O. B. Toon (2004), The impact of humidity above stratiform clouds on indirect aerosol climate forcing, *Nature*, *432*, 1014–1017.

Albrecht, B. A. (1989), Aerosols, cloud microphysics, and fractional cloudiness, *Science*, *245*, 1227–1230.

Albrecht, B. A., C. S. Bretherton, D. Johnson, W. H. Scubert, and A. S. Firsch (1995), The Atlantic stratocumulus transition experiment—ASTEX, *Bull. Am. Meteorol. Soc.*, *76*, 889–904.

Anderson, T. L., R. J. Charlson, D. M. Winker, J. A. Ogren, and K. Holmén (2003), Mesoscale variations of tropospheric aerosols, *J. Atmos. Sci.*, *60*, 119–136.

Bevington, P. R. (1969), *Data Reduction and Error Analysis for the Physical Sciences*, Mcgraw-Hill, New York.

Brenguier, J.-L., P. Y. Chuang, Y. Fouquart, D. W. Johnson, F. Parol, H. Pawlowska, J. Pelon, L. Schüller, F. Schröder, and J. Snider (2000a), An overview of the ACE-2 CLOUDYCOLUMN closure experiment, *Tellus, Ser. B*, *52*, 815–827.

Brenguier, J.-L., H. Pawlowska, L. Schüller, R. Preusker, J. Fischer, and Y. Fouquart (2000b), Radiative properties of boundary layer clouds: Droplet effective radius versus number concentration, *J. Atmos. Sci.*, *57*, 803–821.

Clarke, A. D., et al. (2002), INDOEX aerosol: A comparison and summary of chemical, microphysical, and optical properties observed from land, ship, and aircraft, *J. Geophys. Res.*, *107*(D19), 8033, doi:10.1029/2001JD000572.

Coakley, J. A., Jr., and C. D. Walsh (2002), Limits to the aerosol indirect radiative effect derived from observations of ship tracks, *J. Atmos. Sci.*, *59*, 668–680.

Coakley, J. A., Jr., W. R. Tahnk, A. Jayaraman, P. K. Quinn, C. Devaux, and D. Tanré (2002), Aerosol optical depths and direct radiative forcing for INDOEX derived from AVHRR: Theory, *J. Geophys. Res.*, *107*(D19), 8009, doi:10.1029/2000JD000182.

Coakley, J. A., Jr., M. A. Friedman, and W. R. Tahnk (2005), Retrievals of cloud properties for partly cloudy imager pixels, *J. Atmos. Oceanic Technol.*, *22*, 3–17.

Feichter, J., E. Roeckner, U. Lohmann, and B. Liepert (2004), Nonlinear aspects of the climate response to greenhouse gas and aerosol forcing, *J. Clim.*, *17*, 2384–2398.

Han, Q., W. B. Rossow, and A. A. Lacis (1994), Near-global survey of effective droplet radii in liquid water clouds using ISCCP data, *J. Clim.*, *7*, 465–497.

Hess, M., P. Koepke, and I. Schult (1998), Optical properties of aerosols and clouds: The software package OPAC, *Bull. Am. Meteorol. Soc.*, *79*, 831–844.

Ignatov, A., P. Minnis, N. Loeb, B. Wielicki, W. Miller, S. Sun-Mack, D. Tanré, L. Remer, I. Laszlo, and E. Geier (2005), Two MODIS aerosol products over ocean on the Terra and Aqua CERES SSF datasets, *J. Atmos. Sci.*, *62*, 1008–1031.

Intergovernmental Panel on Climate Change (2001), *Climate Change 2001: The Scientific Basis*, edited by J. T. Houghton et al., Cambridge Univ. Press, New York.

Johnson, D. W., et al. (2000), An overview of the Lagrangian experiments undertaken during the North Atlantic regional Aerosol Characterization Experiment (ACE-2), *Tellus, Ser. B*, *52*, 290–320.

Kaufman, Y. J., and R. S. Fraser (1997), The effect of smoke particles on clouds and climate forcing, *Science*, *277*, 1636–1639.

Kaufman, Y. J., and T. Nakajima (1993), Effect of Amazon smoke on cloud microphysics and albedo—Analysis from satellite imagery, *J. Appl. Meteorol.*, *32*, 729–744.

Kidwell, K. B. (1995), *NOAA Polar Orbiter Data User's Guide*, NOAA Natl. Environ. Satell., Data, and Inf. Serv., Washington, D. C.

King, M. D., W. P. Menzel, Y. J. Kaufman, D. Tanré, B.-C. Gao, S. Platnick, S. A. Ackerman, L. A. Remer, R. Pincus, and P. A. Hubanks (2003), Cloud and aerosol properties, precipitable water, and profiles of temperature and water vapor from MODIS, *IEEE Trans. Geosci. Remote Sens.*, *41*, 442–458.

Kütz, S., and R. Dubois (1997), Balloon-borne aerosol measurements in the planetary boundary layer: Particle production associated with a continental stratiform cloud, *Contrib. Atmos. Phys.*, *70*, 109–116.

Lelieveld, J., and J. Heintzenberg (1992), Sulfate cooling effect on climate through in-cloud oxidation of anthropogenic SO_2, *Science*, *258*, 117–120.

Loeb, N. G., and N. Manalo-Smith (2005), Top-of-atmosphere direct radiative effect of aerosols over global oceans from merged CERES and MODIS observations, *J. Clim.*, *18*, 3506–3526.

Lohmann, U., and J. Feichter (1997), Impact of sulfate aerosols on albedo and lifetime of clouds: A sensitivity study with the ECHAM4 GCM, *J. Geophys. Res.*, *102*(D12), 13,685–13,700.

Lohmann, U., and G. Lesins (2002), Stronger constraints on the anthropogenic indirect aerosol effect, *Science*, *298*, 1012–1015.

Lohmann, U., J. Feichter, J. Penner, and R. Leaitch (2000), Indirect effect of sulfate and carbonaceous aerosols: A mechanistic treatment, *J. Geophys. Res.*, *105*(D10), 12,193–12,206.

Nakajima, T., A. Higurashi, K. Kawamoto, and J. E. Penner (2001), A possible correlation between satellite-derived cloud and aerosol microphysical parameters, *Geophys. Res. Lett.*, *28*, 1171–1174.

Platnick, S., P. A. Durkee, K. Nielson, J. P. Taylor, S.-C. Tsay, M. D. King, R. J. Ferek, P. V. Hobbs, and J. W. Rottman (2000), The role of background cloud microphysics in the radiative formation of ship tracks, *J. Atmos. Sci.*, *57*, 2607–2624.

Platnick, S., M. D. King, S. A. Ackerman, W. P. Menzel, B. A. Baum, J. C. Riédi, and R. A. Frey (2003), The MODIS cloud products: Algorithms and examples from Terra, *IEEE Trans. Geosci. Remote Sens.*, *41*, 459–473.

Podgorny, I. A. (2003), Three-dimensional radiative interactions in a polluted broken cloud system, *Geophys. Res. Lett.*, *30*(14), 1771, doi:10.1029/2003GL017287.

Potter, G. L., and R. D. Cess (2004), Testing the impact of clouds on the radiation budgets of 19 atmospheric general circulation models, *J. Geophys. Res.*, *109*, D02106, doi:10.1029/2003JD004018.

Press, W. H., S. A. Teukolsky, W. T. Vetterling, and B. P. Flannery (1994), *Numerical Recipes in FORTRAN: The Art of Scientific Computing*, 2nd ed., Cambridge Univ. Press, New York.

Quaas, J., O. Boucher, and F.-M. Bréon (2004), Aerosol indirect effects in POLDER satellite data and the Météorologie Dynamique—Zoom (LMDZ) general circulation model, *J. Geophys. Res.*, *109*, D08205, doi:10.1029/2003JD004317.

Raes, F., T. Bates, F. McGovern, and M. Van Liedekerke (2000), The 2nd aerosol characterization experiment (ACE-2): General overview and main results, *Tellus, Ser. B*, *52*, 111–125.

Randall, D., M. Khairoutdinov, A. Arakawa, and W. Grabowski (2003), Breaking the cloud parameterization deadlock, *Bull. Am. Meteorol. Soc.*, *84*, 1547–1564.

Rotstayn, L. D. (1999), Indirect forcing by anthropogenic aerosols: A global climate model calculation of the effective-radius and cloud-lifetime effects, *J. Geophys. Res.*, *104*(D8), 9369–9380.

Rotstayn, L. D., and J. E. Penner (2001), Indirect aerosol forcing, quasi forcing, and climate response, *J. Clim.*, *14*, 2960–2975.

Seinfeld, J. H., and S. N. Pandis (1998), *Atmospheric Chemistry and Physics: From Air Pollution to Climate Change*, John Wiley, Hoboken, N. J.

Sekiguchi, M., T. Nakajima, K. Suzuki, K. Kawamoto, A. Higurashi, D. Rosenfeld, I. Sano, and S. Mukai (2003), A study of the direct and indirect effects of aerosols using global satellite data sets of aerosol and cloud parameters, *J. Geophys. Res.*, *108*(D22), 4699, doi:10.1029/2002JD003359.

Szczodrak, M., P. H. Austin, and P. B. Krummel (2001), Variability of optical depth and effective radius in marine stratocumulus clouds, *J. Atmos. Sci.*, *58*, 2912–2926.

Tahnk, W. R., and J. A. Coakley Jr. (2001a), Improved calibration coefficients for NOAA-14 AVHRR visible and near-infrared channels, *Int. J. Remote Sens.*, *22*, 1269–1283.

Tahnk, W. R., and J. A. Coakley Jr. (2001b), Updated calibration coefficients for NOAA-14 AVHRR channels 1 and 2, *Int. J. Remote Sens.*, *22*, 3053–3057.

Twomey, S. (1974), Pollution and the planetary albedo, *Atmos. Environ.*, *8*, 1251–1256.

Wetzel, M. A., and L. L. Stowe (1999), Satellite-observed patterns in stratus microphysics, aerosol optical thickness, and shortwave radiative forcing, *J. Geophys. Res.*, *104*(D24), 31,287–31,299.

Winker, D. M., J. R. Pelon, and M. P. McCormick (2003), The *CALIPSO* mission: Spaceborne lidar for observation of aerosols and clouds, *Proc. SPIE Int. Soc. Opt. Eng.*, *4839*, 1–11.

————————————

J. A. Coakley Jr., M. A. Matheson, and W. R. Tahnk, College of Oceanic and Atmospheric Sciences, 104 COAS Admin Building, Oregon State University, Corvallis, OR 97331-5503, USA. (coakley@coas.oregonstate.edu)